



Cite this: *J. Mater. Chem. C*, 2015, **3**, 3552

## The development of a wideband and angle-insensitive metamaterial filter with extraordinary infrared transmission for micro-thermophotovoltaics

D. Y. Jiang,<sup>a</sup> W. M. Yang,<sup>\*a</sup> Y. J. Liu,<sup>b</sup> H. L. Liu<sup>c</sup> and J. H. Teng<sup>\*b</sup>

Since the performance of the micro-thermophotovoltaic (TPV) system is significantly limited by the mismatch between the radiation spectrum and the photovoltaic (PV) bandgap, for the first time, a wideband and angle-insensitive metamaterial filter was developed and optimized to address this issue. The developed filter was placed between the reactor and the PV cell and it was able to effectively transmit the valuable photons for power generation and reflect the worthless energy, thus offering great potential to improve the performance of the micro-TPV system. In particular, the filter is applicable for the entire near infrared wavelength range and exhibits extraordinary transmission. For the working wavelength applied in this paper, the obtained peak transmission coefficient from experiments is up to 88.3%. Furthermore, the efficiency of the micro-TPV system is also predicted to be enhanced more than twice with the metamaterial filter applied. Both the experimental and theoretical results show that the incorporation of the metamaterial filter with low bandgap PV cells can be a promising approach to improve the efficiency of the existing micro-TPV system.

Received 16th December 2014,  
Accepted 22nd February 2015

DOI: 10.1039/c4tc02892a

www.rsc.org/MaterialsC

### Introduction

The combustion-driven micro-TPV system has attracted much attention for power generation in portable devices due to its superior energy density compared to the chemical batteries.<sup>1–3</sup> A high performance filter is one of the key components in such a system, which transmits the photons with energy greater than the bandgap of the PV diodes as well as reflects the photons with energy not sufficient to generate charge carriers in the PV cells.<sup>4,5</sup> In the past decade, both selective emitters<sup>6,7</sup> and infrared filters<sup>8,9</sup> have been developed to reshape the radiation spectrum based on rare-earth oxides,<sup>10,11</sup> photonic crystals<sup>12–14</sup> and metamaterials.<sup>15,16</sup> However, the reported selective emitters and filters still face the challenges of material availability, efficient spectral control in the long wavelength range,<sup>17–19</sup> thermal stability<sup>20,21</sup> and angle independency.<sup>22,23</sup> The extraordinary optical transmission (EOT)<sup>24</sup> phenomenon has been observed in the coaxial ring array,<sup>25</sup> which is mainly due to the cylindrical surface plasmon (CSP), planar surface plasmon

(PSP) resonances<sup>26–28</sup> and constructive interference. Besides, the optical response of the coaxial ring array is also insensitive to the incidence angle.<sup>29</sup> Hence, these two features make the coaxial ring array a perfect candidate for high-efficiency spectral control in the optical wavelength range. Here, we demonstrate the suitability of the similar extraordinary transmission phenomenon and other superior features of the coaxial ring array structure in the infrared region and its further application in the micro-TPV system. In addition, the energy transfer process of the micro-TPV system with the coaxial ring array filter applied is also predicted in detail.

The spectral radiance profiles for the blackbody and the reactor at the temperature of 1500 K are shown in Fig. 1. The reactor spectral radiance is calculated by the blackbody spectral radiance multiplied by the spectral emissivity of the reactor material, such as SiC.<sup>30</sup> For a GaSb PV cell which has the cut-off wavelength of 1720 nm, the spectral radiance with the wavelength lower than 1720 nm is capable of generating power through the PV cell, while the spectral radiance with the wavelength higher than 1720 nm is useless. In this case, an ideal filter should have the features as shown in the green line in Fig. 1, which transmits the photons with the wavelength shorter than 1720 nm totally, but reflects the photons with the wavelength greater than 1720 nm. Fig. 2(a) illustrates the schematic of a high-efficiency micro-TPV system with the metamaterial filter which is deposited on the top of the PV cell. The micro-reactor is fueled by hydrogen/hydrocarbon

<sup>a</sup> Department of Mechanical Engineering, National University of Singapore, 9 Engineering Drive 1, 117576, Singapore. E-mail: mpeywm@nus.edu.sg

<sup>b</sup> Institute of Materials Research and Engineering, Agency for Science, Technology and Research (A\*STAR), 3 Research Link, 117602, Singapore. E-mail: jh-teng@imre.a-star.edu.sg

<sup>c</sup> Centre for Disruptive Photonic Technologies, Nanyang Technological University, 637371, Singapore

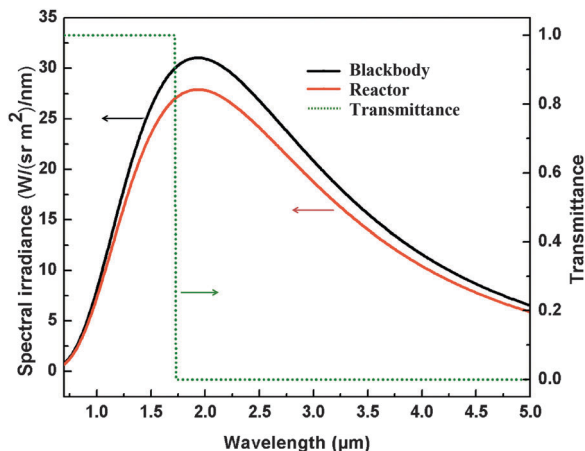


Fig. 1 Black body (black line) and reactor (yellow line) spectral radiances, as well as the ideal filter transmission performance (green line).

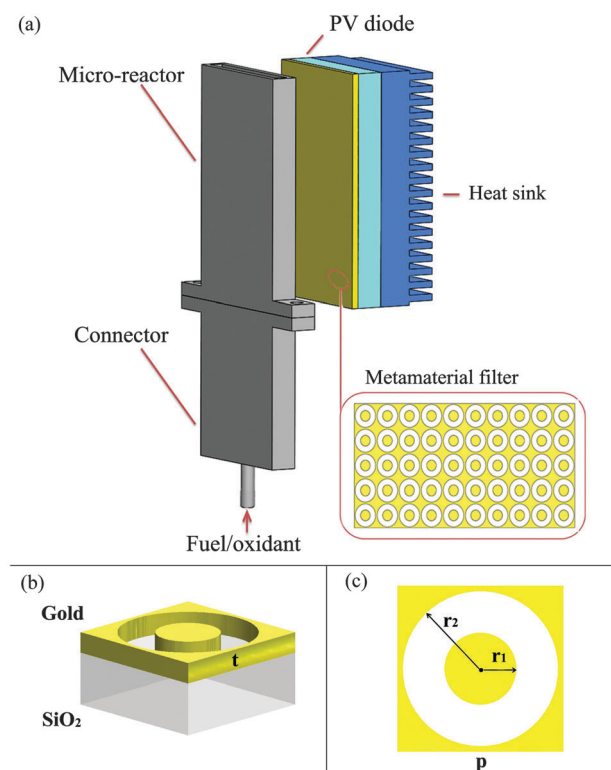


Fig. 2 (a) Schematic of the micro-TPV system with the metamaterial filter. (b) Isometric and (c) top views of one unit cell of the coaxial ring structure, with metal thickness  $t$ , inner radius  $r_1$ , outer radius  $r_2$  and period  $p$ .

and its wall temperature varies from 1000–1500 K.<sup>31,32</sup> When the combustion occurs, the photons from the reactor wall pass through the metamaterial filter towards the PV cells, with electron–hole pairs being produced for power generation. Various low bandgap PV cells, such as GaSb (0.72 eV)<sup>33</sup> and InGaAsSb (0.5–0.55 eV),<sup>34,35</sup> could be used in the micro-TPV system. The attached heat sink is utilized to suppress the temperature of the PV cells.<sup>36</sup> In the real applications, the metamaterial filter and PV cells as well as the heat sink can be installed on both sides of the micro-reactor

to ensure more power generation. Fig. 2(b) and (c) show the detailed coaxial ring structure. The gold pattern is deposited on the amorphous quartz substrate, where its thickness is  $t$ , the inner radius is  $r_1$ , the outer radius of the ring is  $r_2$ , and the period of a unit cell is  $p$ .

The metamaterial filter was realized both in experiments and numerical simulation. At the beginning, a layer of diluted PMMA was deposited on the top of a quartz substrate. The coaxial ring array was fabricated by E-beam lithography. A total area of  $50 \times 50 \mu\text{m}^2$  was fabricated, followed by the deposition of gold. The sample was finally obtained by removing the photoresist through a lift-off process. The transmission and reflection were characterized using a UV-Vis-NIR microspectrometer (CRAIC QDI 2010). The coaxial ring structure was modeled by FDTD simulation. A plane wave source was employed with different incidence angles. The periodic boundaries were applied for the  $x$  and  $y$  directions and a perfectly matched layer (PML) was applied for the  $z$  direction. Two power monitors were set to be 300 nm above and below the Au layer to collect the transmittance and reflectance, respectively.

## Filters for different PV cells

In order to meet the demands for the micro-TPV systems with different bandgaps of PV cells, the passband of the metamaterial filter should be adjustable. The arrays of coaxial rings are found to have such features in the optical wavelength range<sup>37</sup> both in numerical simulation and experiments. The shift of the extraordinary transmittance peak is based on the period variation as predicted by eqn (1),<sup>25</sup> in which  $\lambda$  is the wavelength,  $p_x$  and  $p_y$  are the periods of the coaxial ring along the  $x$  and  $y$  directions,  $i$  and  $j$  are integers,  $\epsilon_m$  and  $\epsilon_d$  are the permittivities of the metal and the dielectric, respectively. It is easy to find that the extraordinary transmittance peak is proportional to the period of the coaxial ring.

$$\lambda = \frac{p_x p_y}{\sqrt{i^2 p_y^2 + j^2 p_x^2}} \sqrt{\frac{\epsilon_m \epsilon_d}{\epsilon_m + \epsilon_d}} \quad (1)$$

Fig. 3 illustrates the transmittance and reflectance of the metamaterial filter with the period of 600 and 900 nm, respectively. The SEM images of the two structures with 600 and 900 nm periods are shown in the inset of Fig. 3(a). A good agreement is achieved between the numerical and experimental results, and the peak transmittance value and the subsequent decay are successfully predicted. It is found that a high transmittance is achieved in the wavelength range of 1100–2000 nm for  $p = 600$  nm, while 1250–2750 nm for  $p = 900$  nm. The measured normalized-to-area peak transmittance for  $p = 600$  nm and  $p = 900$  nm is 1.79 and 1.91, which implies that the extraordinary transmittance occurs in the infrared wavelength range.<sup>38</sup> The low transmittance of the wavelength lower than 1000 nm will not significantly affect the system efficiency. This is due to the fact that there is only a small amount of energy located in this wavelength range, as shown in Fig. 2. A significant feature in Fig. 3 is that the prominent peaks of both transmittance and reflectance red-shifted as the

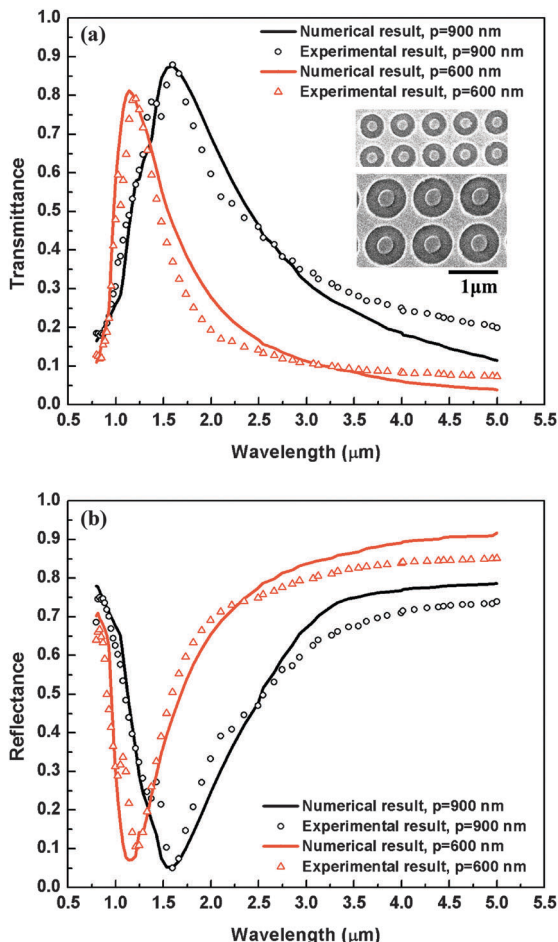


Fig. 3 Transmittance (a) and reflectance (b) of the coaxial ring array with the period of 600 nm ( $t = 50$  nm,  $r_1 = 100$  nm,  $r_2 = 220$  nm) and 900 nm ( $t = 50$  nm,  $r_1 = 140$  nm,  $r_2 = 360$  nm). The inset of (a) shows the SEM images of the designs with 600 nm (top) and 900 nm (bottom) periods.

period increased from 600 to 900 nm. It should be noted that the cut-off wavelength of the filter with  $p = 600$  nm, which can match the cut-off wavelength of the InGaAsSb PV cells (2345 nm) very well. For the PV cells such as InAsSbP<sup>39</sup> with even lower energy bandgaps of 0.45–0.48 eV, the metamaterial filter with larger periods could be employed.

Besides, it is also found that the transmission peak could be red-shifted by decreasing the ring size in the optical wavelength range.<sup>27,37</sup> This phenomenon could also be observed in the infrared wavelength range. Fig. 4 shows two designs, which have the identical metal thickness  $t$ , outer diameter of the ring  $r_2$  and period  $p$ , but a different inner diameter of the ring  $r_1$ . It is found that the design with a larger  $r_1$  value indicating a lower gap size has a red-shifted transmittance profile in comparison with the design with a lower  $r_1$  value. This might be attributed to the enhancements at long wavelengths to TE<sub>1</sub> guided modes of individual coaxial rings.<sup>40</sup>

## Wideband and angle-insensitive filters

To meet the demand for the micro-TPV system, the metamaterial filter should also possess a wide passband, *i.e.*, maintain a high

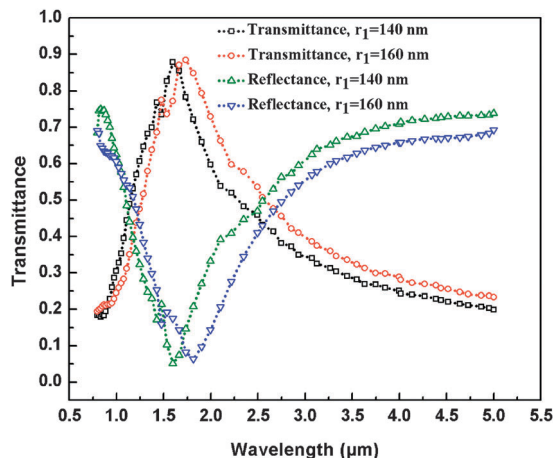


Fig. 4 Measured transmittance and reflectance of coaxial ring arrays with  $r_1$  of 140 nm ( $t = 50$  nm,  $r_2 = 360$  nm,  $p = 900$  nm) and 160 nm ( $t = 50$  nm,  $r_2 = 360$  nm,  $p = 900$  nm), respectively.

transmittance in a relatively long wavelength range. This property could be achieved by adjusting the thickness of the array of coaxial rings. With reference to ref. 25 and 26, two CSP induced transmittance peaks exist in the working wavelength range with the increase of metal thickness. The position of the red peak (at longer wavelength) is independent of the thickness of the array of coaxial rings. However, with the increase of thickness, the position of the blue peak (at lower wavelengths) moves towards the far-infrared direction. The movement of the blue peak causes the fluctuation at the wavelength between 500–1000 nm. This is mainly because of the decrease of the resonant frequency of the cylindrical surface plasmon mode at the increased metal thickness. When the two peaks merge, the wideband transmittance with high intensity would be achieved. This is favorable for the application in the micro-TPV system. Fig. 5(a) and (b) depict the transmittance and reflectance of the coaxial ring array with the metal thickness  $t$  of 250, 300, 350 and 400 nm, respectively. It is obvious that the left transmittance peak red-shifts with the increase of the metal thickness. Besides, the value of the left peak increases simultaneously. Expectedly, the red peaks show weak dependence on the metal thickness. However, their intensities decrease slightly with the increase of  $t$ , which is mainly the result of losses.<sup>26</sup>

As the reactor wall is a diffuse surface, it emits photons towards the hemisphere. In this case, the incidence angle dependence becomes a key parameter to evaluate the performance of the metamaterial filter. Both numerical and experimental studies were performed to identify the incidence angle dependence of the coaxial ring array. Fig. 6 shows the average transmittance at FWHM (full width at half maximum). It is found that the predicted transmittance only decreases slightly with the increase of incidence angles. Compared to experimental results, the measured transmittance has a reasonable agreement with the predicted value. It is difficult to obtain the reflectance with different incidence angles experimentally. This is due to the difficulty in collecting the reflected photons using the detector as the detector area is small

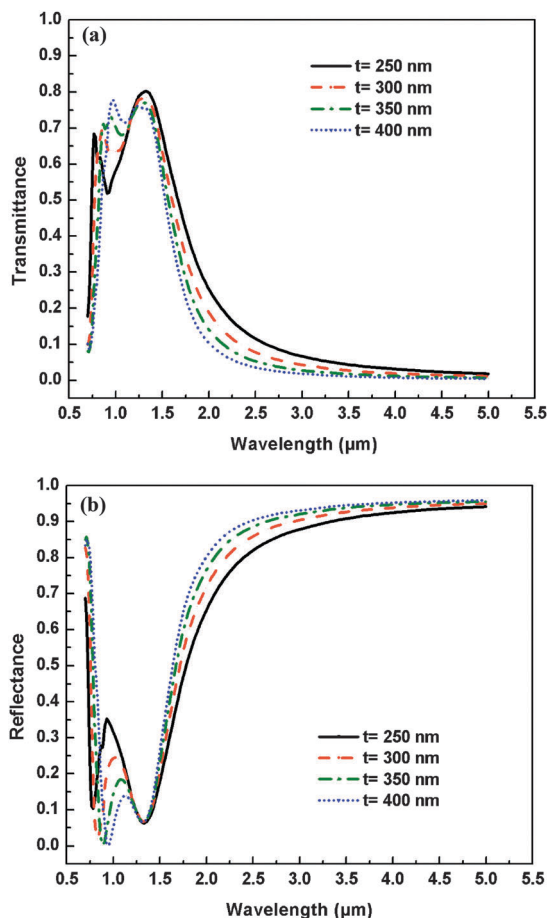


Fig. 5 Predicted transmittance (a) and reflectance (b) of the samples with different metal thicknesses  $t = 250, 300, 350$  and  $400$  nm, respectively.

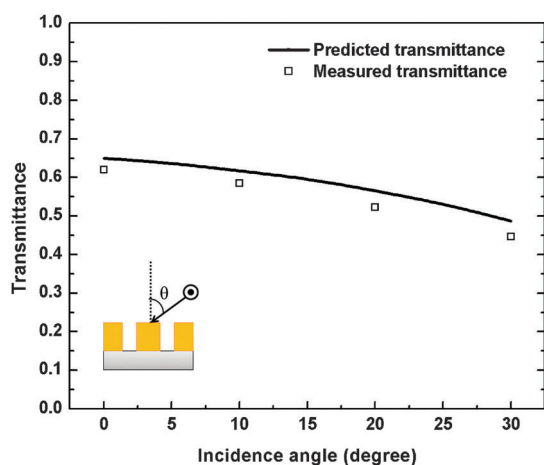


Fig. 6 Measured and predicted average transmittances at FWHM varying with different incidence angles. ( $t = 50$  nm,  $r_1 = 80$  nm,  $r_2 = 220$  nm, and  $p = 600$  nm).

and the distance between the sample and the detector is large. However, in the real micro-TPV application, the reactor wall can play the role of a detector. Therefore, due to the relatively large area of the reactor and the shorter reactor-filter distance, this

phenomenon would have little effect on the performance of the micro-TPV system.

## Micro-TPV systems with metamaterial filters

The effect of the metamaterial filter on the performance of the micro-TPV system is predicted. Fig. 7 depicts the energy conversion process of the system. When the combustion occurs in the micro-reactor, the reactor wall starts emitting photons towards the hemisphere. The photons with the radiation energy within the passband of the metamaterial filter pass through while those out of the passband are reflected. The photons passing through the filter are used for power generation while the reflected photons are useful for improving the temperature of the micro-reactor. However, a small amount of energy may be absorbed using the filter and emitted to the environment, resulting in an energy loss. Therefore, the system efficiency is finally determined by the efficiencies of the reactor, the filter and the PV cell as shown in eqn (2).<sup>41</sup> In order to study the energy transfer at each component, eqn (2) could be written in the form of eqn (3). In which  $E_{\text{emission}}$  is the radiation energy from the reactor wall,  $E_{\text{input}}$  is the chemical energy from hydrogen,  $E_{\text{pass}}$  is the radiation energy passing through the filter and  $P_{\text{generation}}$  is the power generation from the PV cell.

$$\eta_{\text{TPV}} = \eta_{\text{reactor}} \eta_{\text{filter}} \eta_{\text{PV}} \quad (2)$$

$$\eta_{\text{TPV}} = \frac{E_{\text{emission}}}{E_{\text{input}}} \cdot \frac{E_{\text{pass}}}{E_{\text{emission}}} \cdot \frac{P_{\text{generation}}}{E_{\text{pass}}} \quad (3)$$

In order to predict the performance of the metamaterial filter in the micro-TPV system, Ansys Fluent is employed to investigate the energy transfer processes between the micro-reactor and

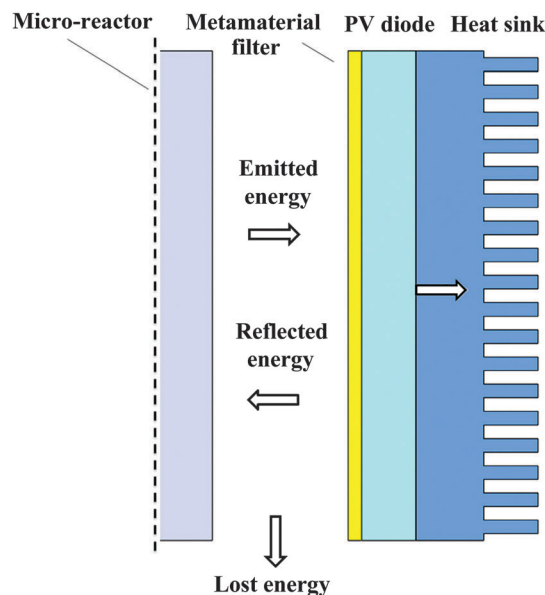


Fig. 7 Energy conversion process of the micro-TPV system with the metamaterial filter.

the filter. A 3D model is established for the micro-reactor, the filter and the air between them. The dimensions of the reacting fluid are 10 mm (length), 1 mm (width) and 18 mm (height), while the reactor wall has a thickness of 0.5 mm. The filter with the dimensions of 10 mm × 18 mm is parallel to the front surface of the reactor wall. The H<sub>2</sub>-air premixed flame is employed as the reacting fluid and modeled by a detailed chemical reaction mechanism with 9 species and 19 steps.<sup>42,43</sup> The discrete ordinates (DO) model is utilized to study the radiative heat transfer between the reactor wall and the filter. The air flow between the reactor wall and the filter is set to be natural convection. The transmittance and reflectance of the filter are obtained from the predicted results as shown in Fig. 3 ( $p = 600$  nm) by taking incidence angles (0–50°) into account. The H<sub>2</sub>-air inlet flow velocity varies from 3–5 m s<sup>-1</sup>, while the distance between the front reactor wall and the filter is set to be 1, 2 and 3 mm, respectively.

Four cases are compared to evaluate the performance of the metamaterial filter. In case A, no metamaterial filter is installed on top of the PV cell, while the metamaterial filters are employed for cases B, C, and D, where the distances between the filter and the reactor wall for cases A, B, C, and D are 1, 1, 2 and 3 mm, respectively. In order to ensure the four cases to be comparable, the input energies of hydrogen are the same. Fig. 8 illustrates the reactor wall temperature distributions for the cases A, B, C and D, respectively. As shown in Fig. 8(a), the highest reactor wall temperature is obtained in case B, followed by case C, case D and case A. Compared with that of case A, the higher reactor wall temperatures of case B, C and D can be attributed to the reflected energy from the metamaterial filters. Compared with case B, the relatively low reactor wall temperatures of case C and D are caused by the increased reactor-filter distance, which leads to a smaller view factor. With the increase of the flow velocity to 4 and 5 m s<sup>-1</sup> (see Fig. 8(b) and (c)), the reactor wall temperature is found to be even higher. This is because more hydrogen is brought in and more chemical energy is released.

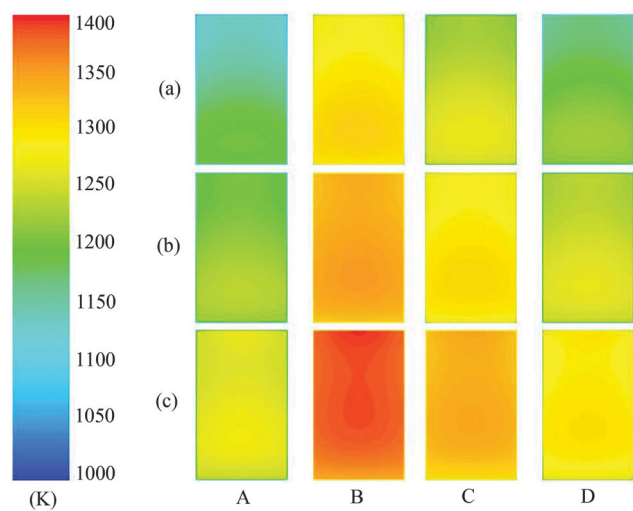


Fig. 8 Reactor wall temperature distributions at (a) 3 m s<sup>-1</sup>, (b) 4 m s<sup>-1</sup> and (c) 5 m s<sup>-1</sup>. (Case A, without the filter; cases B–D with the filter and their reactor-filter distances are 1, 2 and 3 mm, respectively.)

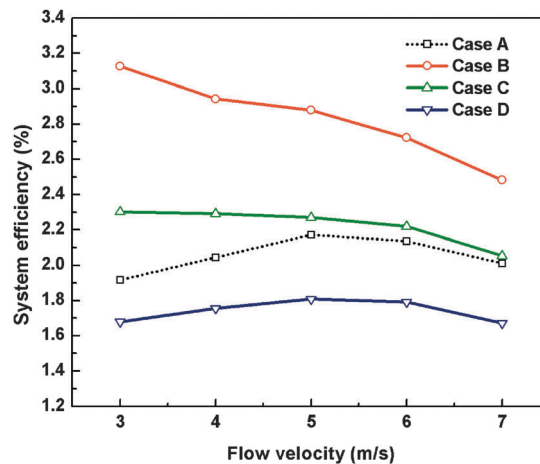


Fig. 9 Predicted system efficiencies of the micro-TPV system with different inlet flow velocities for the four cases. (Case A, without the filter; case B, with the filter and the reactor-filter distance of 1 mm; case C, with the filter and the reactor-filter distance of 2 mm; case D, with the filter and the reactor-filter distance of 3 mm) Lines connecting the symbols are only for the sake of visualization.

The predicted system efficiencies for the four cases are shown in Fig. 9 when the inlet flow velocity varies from 3–7 m s<sup>-1</sup>. As shown in eqn (2), the micro-TPV system efficiency is determined by the efficiencies of the reactor, the filter and PV cells. In this paper, the GaSb PV cell is employed for calculation and the efficiency is adopted from the study by Yang *et al.*<sup>44</sup> As observed in Fig. 9, the system efficiency of case A increases when the flow velocity increases from 3–5 m s<sup>-1</sup> but decreases when the flow velocity further increases from 5–7 m s<sup>-1</sup>. As there is no filter applied in this case, the system efficiency would only be determined by the efficiencies of the reactor and PV cells. The initial increase could be attributed to the increased reactor wall temperature, which is caused by the more heat release. From Wien's displacement law, the spectral irradiance would blue-shift when the source temperature increases. By this mechanism, more energy could be converted into electricity, and the system efficiency for case A increases. However, the efficiency decrease when the inlet flow velocity increases from 5 m s<sup>-1</sup> onwards could be due to the large amount of energy loss from the exhaust because of incomplete combustion. By employing filters for cases B, C and D, the filter efficiencies decrease. However, the employment of the filter increases the efficiencies of the reactor and PV cells simultaneously. This is the reason why the system efficiency of case B is higher than that of case A. With the increase of the reactor-filter distance, more energy loss is incurred by the reduced view factor. As a result, the reflected photons could not be collected using the reactor effectively. This will lead to the decrease of reactor efficiency and wall temperature. The decreased reactor wall temperature results in a reduced PV cell efficiency at the same time because of the red-shift of the radiation profile. As a result, the system efficiency for cases C and D are lower than that of case B. These results imply that the performance of a filter is not only judged by the transmittance, but also by the reflectance.

## Conclusions

The primary objective of this study was to develop a meta-material filter for micro-TPV application. The results showed that the normalized-to-area transmittance is more than unity, which implied that the extraordinary transmission could be achieved in the near infrared wavelength range. To fulfill the demand for the micro-TPV system, the passband could be adjusted by changing the period of the coaxial ring structure and a slight change could also be made by changing the inner radius of the ring. These findings are of crucial importance for the micro-TPV system with different bandgap PV cells. A wide band pass filter was created when the metal thickness  $t$  is increased, which could be attributed to the merging of the two CSP induced transmittance peaks. Besides, the metamaterial filter showed the angle-insensitive feature in its working wavelength range. By increasing the incidence angle from 0 to 30 degrees, the decrease of transmittance is generally very slight. In order to analyze the whole energy conversion process from chemical energy into power generation, the micro-TPV system efficiency was predicted by incorporating the micro-reactor and the PV cell. Compared with the original system, the system efficiency was found to be increased significantly after the metamaterial filter was employed, which should be attributed to the improved performance of the reactor and the PV cell. The developed wideband and angle-insensitive metamaterial filter exhibits many outstanding features and provides great potential to improve the performance of the existing micro-TPV system.

## Acknowledgements

This project is supported by the research grant R-265-000-460-112.

## Notes and references

- W. R. Chan, P. Bermel, R. C. Pilawa-Podgurski, C. H. Marton, K. F. Jensen, J. J. Senkevich, J. D. Joannopoulos, M. Soljačić and I. Celanovic, *Proc. Natl. Acad. Sci. U. S. A.*, 2013, **110**, 5309–5314.
- S. K. Chou, W. M. Yang, K. J. Chua, J. Li and K. L. Zhang, *Appl. Energy*, 2011, **88**, 1–16.
- Y. Ju and K. Maruta, *Prog. Energy Combust. Sci.*, 2011, **37**, 669–715.
- L. C. Chia and B. Feng, *J. Power Sources*, 2007, **165**, 455–480.
- S. Basu, Y. B. Chen and Z. M. Zhang, *Int. J. Energy Res.*, 2007, **31**, 689–716.
- V. Rinnerbauer, A. Lenert, D. M. Bierman, Y. X. Yeng, W. R. Chan, R. D. Geil, J. J. Senkevich, J. D. Joannopoulos, E. N. Wang, M. Soljačić and I. Celanovic, *Adv. Energy Mater.*, 2014, 1400334.
- H. Sai and Y. Kanamori, *Microscale Thermophys. Eng.*, 2003, **7**, 101–115.
- T. Bauer, I. Forbes, R. Penlington and N. Pearsall, *Sol. Energy Mater. Sol. Cells*, 2005, **88**, 257–268.
- I. Celanovic, F. O'Sullivan, M. Ilak, J. Kassakian and D. Perreault, *Opt. Lett.*, 2004, **29**, 863–865.
- A. Licciulli, D. Diso, G. Torsello, S. Tundo, A. Maffezzoli, M. Lomascolo and M. Mazzer, *Semicond. Sci. Technol.*, 2003, **18**, S174.
- G. Torsello, M. Lomascolo, A. Licciulli, D. Diso, S. Tundo and M. Mazzer, *Nat. Mater.*, 2004, **3**, 632–637.
- C. Argyropoulos, K. Q. Le, N. Mattiucci, G. D'Aguanno and A. Alù, *Phys. Rev. B: Condens. Matter Mater. Phys.*, 2013, **87**, 205112.
- J. Fleming, S. Lin, I. El-Kady, R. Biswas and K. Ho, *Nature*, 2002, **417**, 52–55.
- V. Rinnerbauer, S. Ndao, Y. X. Yeng, W. R. Chan, J. J. Senkevich, J. D. Joannopoulos, M. Soljačić and I. Celanovic, *Energy Environ. Sci.*, 2012, **5**, 8815.
- S. Molesky, C. J. Dewalt and Z. Jacob, *Opt. Express*, 2013, **21**, 96–110.
- C. Simovski, S. Maslovski, I. Nefedov and S. Tretyakov, *Opt. Express*, 2013, **21**, 14988–15013.
- S. I. Mostafa, N. H. Rafat and S. A. El-Naggar, *Renewable Energy*, 2012, **45**, 245–250.
- L. Fraas, J. Samaras, H. Huang, L. Minkin, J. Avery, W. Daniels and S. Hui, *TPV generators using the radiant tube burner configuration*, 2001.
- P. Bermel, M. Ghebrehbrhan, W. Chan, Y. X. Yeng, M. Araghchini, R. Hamam, C. H. Marton, K. F. Jensen, M. Soljačić and J. D. Joannopoulos, *Opt. Express*, 2010, **18**, A314–A334.
- X. Liu, T. Tyler, T. Starr, A. F. Starr, N. M. Jokerst and W. J. Padilla, *Phys. Rev. Lett.*, 2011, **107**, 045901.
- B. Zhao, L. Wang, Y. Shuai and Z. M. Zhang, *Int. J. Heat Mass Transfer*, 2013, **67**, 637–645.
- R. T. Kristensen, *J. Appl. Phys.*, 2004, **95**, 4845.
- C. Wu, B. Neuner III, J. John, A. Milder, B. Zollars, S. Savoy and G. Shvets, *J. Opt.*, 2012, **14**, 024005.
- T. W. Ebbesen, H. Lezec, H. Ghaemi, T. Thio and P. Wolff, *Nature*, 1998, **391**, 667–669.
- F. Baida and D. Van Labeke, *Opt. Commun.*, 2002, **209**, 17–22.
- M. Haftel, C. Schlockermann and G. Blumberg, *Phys. Rev. B: Condens. Matter Mater. Phys.*, 2006, **74**, 235405.
- M. I. Haftel, C. Schlockermann and G. Blumberg, *Appl. Phys. Lett.*, 2006, **88**, 193104.
- S. M. Orbons, A. Roberts, D. N. Jamieson, M. I. Haftel, C. Schlockermann, D. Freeman and B. Luther-Davies, *Appl. Phys. Lett.*, 2007, **90**, 251107.
- A. Belkhir and F. Baida, *Phys. Rev. E: Stat., Nonlinear, Soft Matter Phys.*, 2008, **77**, 056701.
- G. Neuer and G. Jaroma-Weiland, *Int. J. Thermophys.*, 1998, **19**, 917–929.
- D. Jiang, W. Yang, K. J. Chua and J. Ouyang, *Appl. Therm. Eng.*, 2013, **61**, 670–677.
- W. Yang, S. Chou, K. Chua, H. An, K. Karthikeyan and X. Zhao, *Appl. Energy*, 2012, **97**, 749–753.
- O. Sulima and A. Bett, *Sol. Energy Mater. Sol. Cells*, 2001, **66**, 533–540.

- 34 O. Sulima, R. Beckert, A. Bett, J. Cox and M. Mauk, *IEE Proc.: Optoelectron.*, 2000, **147**, 199–204.
- 35 M. W. Dashiell, J. F. Beausang, H. Ehsani, G. Nichols, D. M. Depoy, L. R. Danielson, P. Talamo, K. D. Rahner, E. J. Brown and S. R. Burger, *IEEE Trans. Electron Devices*, 2006, **53**, 2879–2891.
- 36 L. Ferguson and L. Fraas, *Sol. Energy Mater. Sol. Cells*, 1995, **39**, 11–18.
- 37 G. Si, Y. Zhao, H. Liu, S. Teo, M. Zhang, T. Jun Huang, A. J. Danner and J. Teng, *Appl. Phys. Lett.*, 2011, **99**, 033105.
- 38 S. G. Rodrigo, *Optical Properties of Nanostructured Metallic Systems*, Springer, Berlin, Germany, 2012.
- 39 A. Popov, V. Sherstnev, Y. Yakovlev, R. Mücke and P. Werle, *Appl. Phys. Lett.*, 1996, **68**, 2790–2792.
- 40 F. I. Baida, D. Van Labeke and B. Guizal, *Appl. Opt.*, 2003, **42**, 6811–6815.
- 41 M. Zenker, A. Heinzl, G. Stollwerck, J. Ferber and J. Luther, *IEEE Trans. Electron Devices*, 2001, **48**, 367–376.
- 42 J. C. Andrae and P. H. Björnbohm, *AIChE J.*, 2000, **46**, 1454–1460.
- 43 V. Giovangigli and M. Smooke, *Combust. Sci. Technol.*, 1987, **53**, 23–49.
- 44 W. M. Yang, S. K. Chou, C. Shu, Z. W. Li and H. Xue, *Sol. Energy Mater. Sol. Cells*, 2003, **80**, 95–104.